AIAA JOURNAL
Vol. 45, No. 5, May 2007

Effects of a Needle on Shrouded Hartmann–Sprenger Tube Flows

Guoping Xia,* Ding Li,† and Charles L. Merkle‡
Purdue University, West Lafayette, Indiana, 47907

DOI: 10.2514/1.18591

A computational analysis of the effects of a needle on a shrouded Hartmann–Sprenger tube driven by a Mach 2 jet is presented. Solutions in the absence of a resonance tube indicate that the "ideally" expanded jet contains a complex, but weak, Mach diamond pattern that is essentially unaffected by placing a needle on the axis. The resonant modes, however, are strongly impacted by a needle. When a needle is not present, a 4-kHz screech mode is generated with an oscillating shock in front of the tube. When a needle is present, the high-frequency modes are suppressed and a quarter-wave (∼570 Hz), regurgitant oscillation is observed. Lengthening the needle causes the high frequencies to decrease gradually and the quarter wave to increase. Needles longer than the nozzle tend to reduce the amplitude. The results are in quantitative agreement with available measurements and the trends are consistent with results for underexpanded converging nozzles.

Nomenclature

c	=	sound speed
D	=	inside diameter of the Hartmann–Sprenger tube
d	=	axial spacing between the nozzle exit and the Hartmann–Sprenger tube inlet
f	=	frequency
L	=	resonant tube length
p	=	static pressure
p^0	=	total pressure
r, R	=	radial coordinate and Hartmann–Sprenger tube radius, respectively
T	=	period of oscillation

I. Introduction

A HARTMANN–SPRENGER (H–S) tube is created by aligning a blind tube with the axis of a jet so that the oncoming flow is directed into its open end, as shown in the top sketch of Fig. 1. Although resonance can be created with either subsonic or supersonic jets, in this figure, we portray a supersonic jet from a converging–diverging (C–D) nozzle. It is not difficult to anticipate that such a configuration can produce resonance wherein in one phase, the jet is swallowed and compresses the gas inside the tube, as shown in the top sketch of Fig. 1, whereas 180 deg later, the compressed gases expand and force the jet to deviate around the tube, as in the middle sketch. An alternate possibility is shown in the bottom sketch of Fig. 1, in which the supersonic jet produces a bow shock outside the tube that induces the flow to deviate around the tube. The resonant flows produced by generic configurations of this nature have attracted the attention of researchers for more than three-quarters of a century. Placing a long, narrow rod (a "needle") on the nozzle centerline, as shown in Fig. 1, has proven to be important for producing oscillations behind ideally expanded supersonic jets and some subsonic jets, but is not needed for underexpanded jets from a convergent nozzle. The focus of the present paper is to ascertain whether a computational model shows the same sensitivity to the presence of a needle and to address, in more detail than is possible in experiments, the character of the resulting flowfield. In particular, we wish to investigate how the needle length affects the transition from the regurgitant mode to a quiescent flow or alternative mode.

High-frequency oscillations were first observed in a pitot tube by Hartmann [1] when traversing the Mach diamond region of a supersonic jet from an underexpanded convergent nozzle. In later investigations, he reported that the fluctuations were produced in regions of positive pressure gradient by the oscillations of a strong normal shock in front of the tube [2]. Sprenger [3] noted that a similar configuration could generate intense heating at the closed end of the tube through the dissipation generated by the sequence of weak shocks successively acting on the gas trapped within the tube. In addition, he noted that subsonic jets could produce heating if a needle were placed along the axis or across the open end of the tube.

Because of these initial investigations, the mechanics of Hartmann–Sprenger tubes have been the subject of numerous experimental and analytical studies. Most have used the nonuniform Mach diamond flowfield downstream of an underexpanded, convergent nozzle [4–7], but resonance has also been generated in subsonic jets [3,8] and in ideally expanded supersonic jets [4,5]. In addition to jet experiments, oscillations have been observed in tubes placed in uniform subsonic [8,9] and supersonic [9] flows. Hartmann–Sprenger tubes have also been considered for specific applications such as using their heat-generation capabilities for rocket engine ignition [10], as fluid actuators for flow control [11–15], or as a pulsating flow source for studying unsteady ejectors [16].

Sarohia and Back [6] showed that a convergent nozzle impinging on an open-ended tube can exhibit three distinct oscillation regimes: a jet instability mode, a jet regurgitant mode, and a jet screech mode. The jet instability mode is observed in subsonic jets and is driven by the periodic vortex structures in the mixing layer of the jet. The frequency of the instability is set by the Strouhal number of vortex formation. Either regurgitant or screech modes are observed in the nonuniform supersonic flowfield created by an underexpanded jet, depending upon the separation distance between the nozzle exit and the open end of the tube and the degree of underexpansion (the pressure ratio) of the flow. The jet screech mode is generated when the tube lies in an "unstable" regime in which the axial pressure gradient is positive, as originally observed by Hartmann [2]. This decelerating supersonic field sets up an oscillating normal shock in front of the tube, as in the bottom sketch of Fig. 1, and drives the ensuing oscillations at a frequency determined by local flow conditions.

The jet regurgitant mode sometimes appears when the tube is outside the unstable regime. In this mode, the jet is alternately

Presented as Paper 3888 at the 33rd AIAA Fluid Dynamics Conference and Exhibit, Orlando, FL, 23–26 June 2003; received 5 July 2005; accepted for publication 22 October 2006.

*Research Associate, School of Mechanical Engineering; xiag@purdue.edu. Member AIAA.
†Senior Researcher, School of Mechanical Engineering. Member AIAA.
‡Reilly Professor of Engineering. Member AIAA.

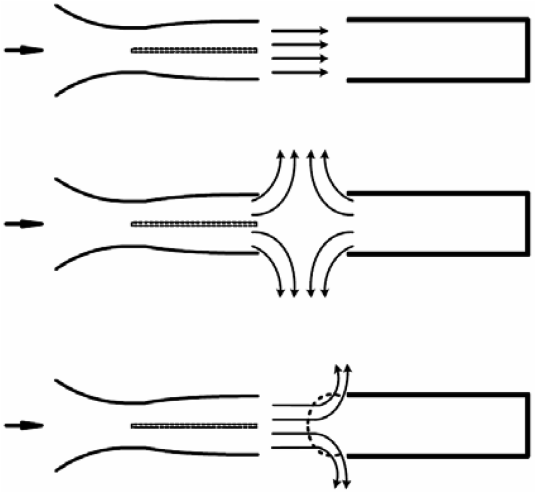

Fig. 1 Schematic diagram of the Hartmann–Sprenger tube showing two possible modes of operation: regurgitant mode (top two) and screech with bow shock (bottom).

swallowed and regurgitated from the tube, thereby driving it at its quarter-wave frequency, as in the top two sketches of Fig. 1. In the first phase, the jet enters the tube and compresses the gas in the tube, causing the pressure inside the tube to increase. This high-pressure gas then expands in the second phase and leaves the tube. The process consists of a compression wave that enters the open end of the tube, traverses its length, reflects off the closed end, and returns to set up a rarefaction wave from the open end. This expansion wave again traverses the tube in both directions, to provide the tube-emptying process. The frequency of this mode corresponds to the tube quarter wave $f = c/4L$.

Although Sarohia and Back [6] indicated that the regurgitant quarter-wave mode is observed only at selected locations in nonuniform supersonic jets, other experimental results [5,8,15] have indicated a much broader occurrence when a needle is placed along the axis. For example, in contrast to Sarohia and Back's results, which exhibited only the jet instability mode in subsonic flows, Sprenger [3] reported a strong regurgitant mode resonance down to a jet Mach number of 0.5, and Brocher and Duport [8] observed regurgitant oscillations at Mach numbers as low as 0.1. Regurgitant quarter-wave oscillations were also observed behind an over-expanded convergent nozzle and an ideally expanded supersonic nozzle [5] when a needle was used. In addition, regurgitant tube oscillations in uniform flows at both subsonic and supersonic Mach numbers were reported by Vrebalovich [9] and Brocher and Duport [8] when a trip was placed upstream of the tube. Clearly, the presence of a thin needle can have a strong influence on the resulting flowfield.

The argument given for this sensitivity to the needle [5] is that the total pressure loss on the centerline arising from needle wake is instrumental in setting up the oscillations. In the absence of a needle, the small entropy increase inside the tube weakens the reflected waves sufficiently that any oscillations decay. Conversely, the energy loss produced by the needle wake enables the reflected wave to overcome the energy of the incoming fluid, leading to amplification and limit cycle oscillations.

Although experimental studies of Hartmann–Sprenger tubes have been reported for many years, computational modeling is relatively recent. Kim and Chang [17], Chang et al. [18], and Ko and Chang [19] presented various aspects of Hartmann–Sprenger tube flows for underexpanded convergent nozzles based upon an Euler equation formulation. Their computations show excellent agreement with experimental shadowgraphs of the region between the nozzle and the jet for the regurgitant flow mode behind an underexpanded convergent nozzle and properly predict both the regurgitant and the jet screech modes [6] at appropriate jet pressure ratios. Their results clearly demonstrate the large difference in the mass inflow and outflow between these two supersonic modes.

Hamed et al. [20,21] presented Navier–Stokes simulations of convergent-nozzle Hartmann–Sprenger tubes. Reference [20] includes simulations with a needle and shows excellent agreement with the experimentally observed quarter-wave frequency and good agreement with measured fluctuation amplitudes. Reference [21] considers a Hartmann–Sprenger tube without a needle at four different jet Mach number conditions. The results show a proper transition from the regurgitant mode to the jet screech mode and also demonstrate the expected transition from the quarter-wave frequency to a broadband high-frequency spectrum at the latter condition.

II. Results and Discussion

The H–S tube geometry considered in the present paper corresponds to the experimental configuration used by Wilson and Paxson [16] to generate a periodic flow to study the entrainment characteristics of unsteady ejectors. The geometry, which is shown in Fig. 2, is composed of a supersonic Mach 2 nozzle, similar to the one used by Brocher, et al. [5], with the Hartmann–Sprenger tube aligned directly above it with the open end at the bottom and the closed end at the top. The external shroud guides the flow around the outer surface of the H–S tube so that it exhausts through the top in the desired unsteady, periodic fashion, as noted in Fig. 2.

The specific dimensions of the device are as follows. The convergent–divergent nozzle that drives the H–S tube has a throat diameter of 0.5 in. and a nozzle exit diameter of 0.652 in.,

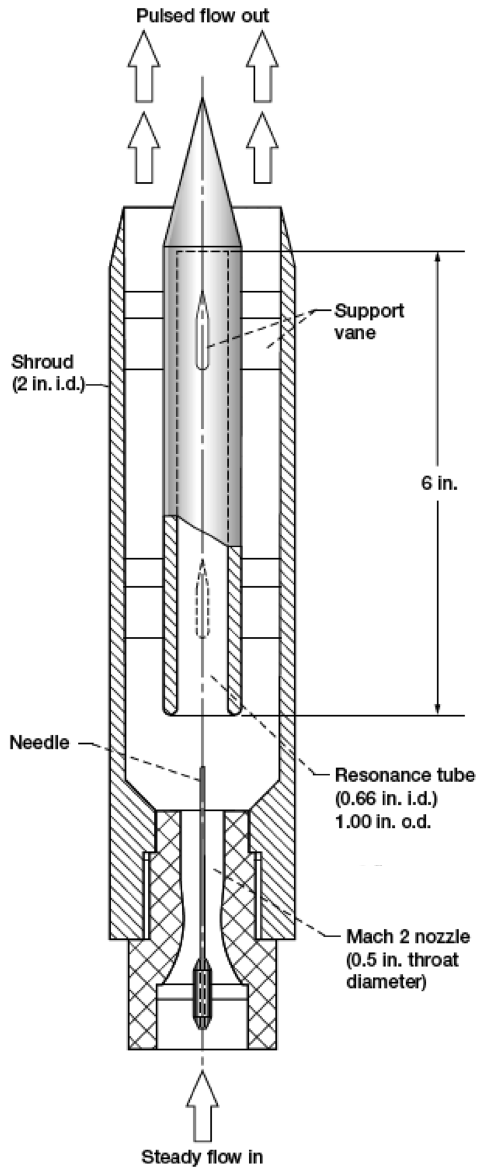

Fig. 2 Shrouded Hartmann–Sprenger tube configuration of Wilson and Paxson [16].

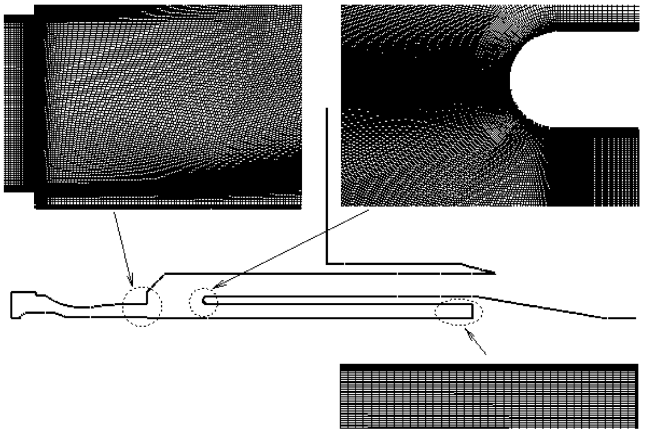

Fig. 3 Computational domain for the calculations, showing details of the local grid at the nozzle exit, the lip of the tube, and the closed end of tube; total grid is 300,000 points.

corresponding to a design Mach number of 2 at the exit. The resonance tube has an inner diameter of 0.66 in., an outer diameter of 1 in., and a length of 6 in. ($L/D = 9$). The open end of the tube is placed approximately two diameters ($d = 1.25$ in.) downstream of the nozzle exit. In the presence of oscillations, the outflow is dominated by a periodic series of ring vortices created by the resonance that provides the desired unsteady flowfield for studying the thrust augmentation characteristics of unsteady ejectors [16].

The sketch in Fig. 2 also indicates that a needle is placed along the axis of the supersonic nozzle to generate oscillations. The diameter of the needle is 0.06 in., resulting in an area blockage of less than 1.5% of the throat area. Parametric studies of the effect of changing the length of this needle are presented, including a reference case when the needle is absent, to deduce its effect on the oscillations. The total pressure of the inlet flow is 7.8 atm and the total temperature is 300 K. When the supporting vanes in the tube are neglected, the flow passage is axisymmetric.

The computational domain shown in Fig. 3 contains the nozzle, the resonance tube, the needle, the tube surrounding the Hartmann–Sprenger tube, and an external domain to allow physically correct behavior at the outflow plane of the device. Representative local sections from a typical grid of approximately 300,000 points are also given. Results from a more refined mesh are also presented to verify grid convergence. The computational domain starts upstream of the nozzle throat and includes a steady flow region inside the supersonic section of the nozzle, as well as the unsteady flow over the remainder of the domain. For computational processing, the mesh was divided into multiple zones for distribution to a PC cluster. The computations were obtained with the unstructured GEMS code [22] using second-order accuracy in time and space and a two-equation k-ω turbulence model [23].

A. Nozzle Flow Characteristics Without Resonant Tube

We begin by characterizing the flow in the supersonic portion of the Mach 2 C–D nozzle and the near-field plume of the jet that is used to drive the H–S tube in the present simulations. The pressure contours of the steady solution in the divergent section and the near-field plume that are produced by the isolated nozzle in the absence of the resonant tube are shown in Fig. 4. The plot at the top left shows the flowfield without a needle, and the one on the right shows the solution with a needle that extends to the exit plane.

The compression from the contoured nozzle wall coalesces to a shock wave near the axis that initiates a diamond pattern both inside and outside the nozzle. The presence of the needle has a minor effect on the location and strength of this pattern. A weak expansion is also initiated at the nozzle exit plane, indicating that the flow is very modestly underexpanded. The two families of waves result in a relatively complicated wave structure, as can be seen in Fig. 4, but it is clear that the needle has no major effect on the flowfield.

The static p and stagnation p^0 pressure distributions along the axial direction at three different radii [$r = 0, 0.1$, and 0.2 in. ($r/R = 0, 0.3$, and 0.6)] are shown on the lower half of Fig. 4. The radial positions of these pressure distribution plots coincide with the axial lines in the top half of the figure. In the case without the needle (on the left), in which the only dissipation comes from the shocks, the total pressure along the radial positions off the axis remains almost constant, whereas the total pressure along the axis decreases in stepwise fashion as it crosses each shock.

In the case in which the needle is present (on the right), the stagnation pressure at the two outer locations ($r/R = 0.3$ and 0.6) look very much like those without the needle. The stagnation pressure on the centerline, however, is very much different from these outer locations or the axis location for the case without the needle. The needle, though very small, reduces the total pressure on the axis to the local static pressure. Downstream of the end of the nozzle, this total pressure on the axis is pumped back up by the surrounding flow, so that it increases with distance. (The total pressure for the $r = 0$ plot begins at the end of the needle.) The total pressure deficit along the axis allows the evacuation of the tube, thereby generating a regurgitant oscillation, as is shown later.

B. Effect of Needle Length on Tube Resonance

To investigate the impact of the needle on tube resonance, we consider five needle configurations, including one case without a needle and four with needles of different lengths. These five configurations are shown in Fig. 5. Starting with configuration 1, neither the needle nor its stem is present. In configuration 2, the

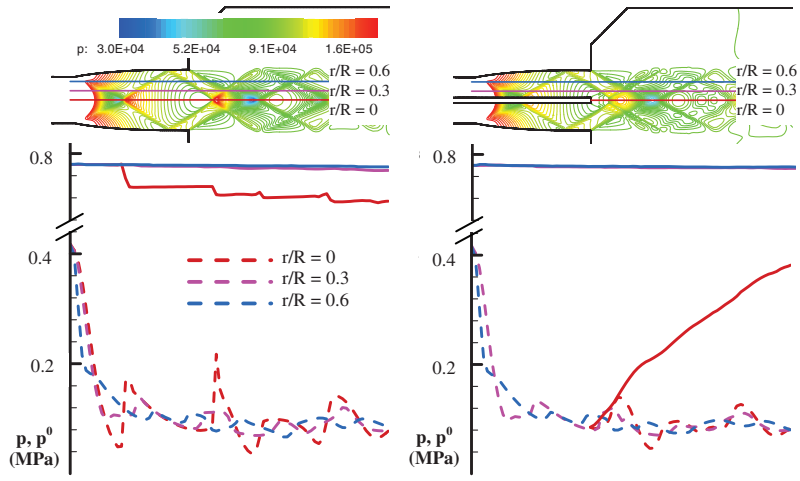

Fig. 4 Free jet pressure contours without a needle (top left) and with a needle (top right); corresponding static and stagnation pressure profiles versus axial distance without a needle (bottom left) and with a needle (bottom right); stagnation pressure (solid line) and static pressure (dashed line).

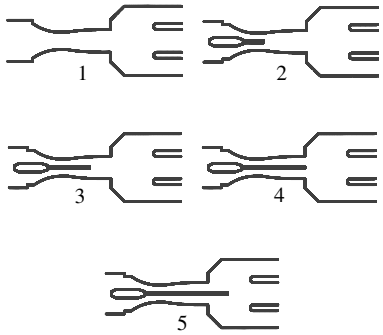

Fig. 5 Different needle configurations: 1) no needle, 2) needle ends at the throat, 3) needle extends to half of the nozzle length, 4) needle extends to the nozzle exit, and 5) needle extends halfway to the tube entrance.

needle ends at the throat, whereas in configuration 3, it extends halfway between the throat and the exit plane. In configuration 4, the needle ends at the exit plane of the nozzle, and in configuration 5, it is extended halfway from the nozzle exit to the resonance-tube inlet. Calculations of the five cases were started from a quasi-steady state and continued until repetitive cycles were obtained.

Figure 6 shows the pressure oscillations on the axis of the resonance tube at the closed end for each of the five needle configurations. When the needle is not present (top curve), a high-frequency oscillation of relatively low amplitude is present. In addition, the presence of a weak longer wavelength (the quarter-wave mode) can also be discerned. In configuration 2 (the needle extends only to the throat), the quarter-wave oscillation becomes more dominant and some of the high-frequency content is lost. As the needle length is extended to the middle and end of the divergent section (configurations 3 and 4), the amplitude of the quarter-wave grows and the high-frequency wave continues to diminish. The oscillation decreases when the needle is stretched beyond the nozzle exit plane (configuration 5). This may suggest that a longer needle can block the path of the evacuation.

Two different sets of results are shown in the fourth frame of Fig. 6, to compare the solution on a grid when the mesh is refined by a factor of 2 in the axial direction with that on the original grid. The results are qualitatively similar, indicating that the grid used in the comparison series is sufficient for capturing the dominant features of the Hartmann–Sprenger tube flows. Note that the solutions are quasi periodic, with minor differences from cycle to cycle, because complete periodicity is never reached. The primary difference between the two grid solutions appears to arise because of period-to-period variations rather than grid resolution.

Fourier analyses of the oscillations in Fig. 6 are shown in Fig. 7, with results for configurations 1 and 2 in the upper plot and those for configurations 3, 4, and 5 in the lower plot. The dominant frequency for the case without the needle (configuration 1) is 4200 Hz, with a second peak at 8400 Hz. The high-frequency modes observed without the needle are indicative of the screech mode and are in qualitative agreement with screech-mode frequencies reported by Sarohia and Back [6] for the convergent-nozzle case.

The quarter-wave frequency (570 Hz) is the dominant mode for all cases with the needle present. In configuration 2, in which the needle ends at the throat, the high-frequency modes remain, but their amplitude is much lower than without the needle. For the longer needles in configurations 3 and 4, the amplitude of the quarter-wave mode is approximately twice its strength as in configuration 2 (and an order of magnitude larger than without the needle), whereas the amplitudes of the higher frequencies are further decreased. The second harmonic (1140 Hz) becomes quite strong in configurations 4 and 5, even though the amplitude of the quarter wave is decreased when the needle is extended beyond the nozzle exit plane. These results clearly show that the needle causes the oscillation to transition from the screech to the regurgitant mode.

The leading frequency in the experimental measurements [16,24] was 550 Hz, based on a needle that extended slightly outside the nozzle. The present predictions of 570 Hz are in excellent agreement with this measurement. In addition, the calculated quarter-wave frequency based on room temperature (300 K) is 565 Hz. Both the comparison with experiment and analyses of the unsteady flow indicate that this quarter-wave frequency corresponds to a regurgitant mode.

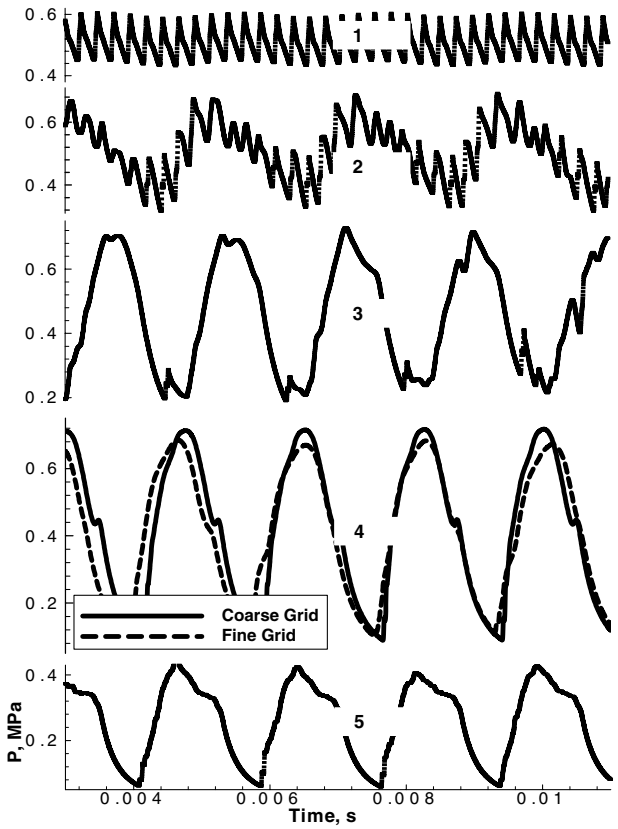

Fig. 6 Pressure oscillation at the closed end of the resonance tube for five different needle configurations shown in Fig. 5; frame 4 compares solutions on two different grids.

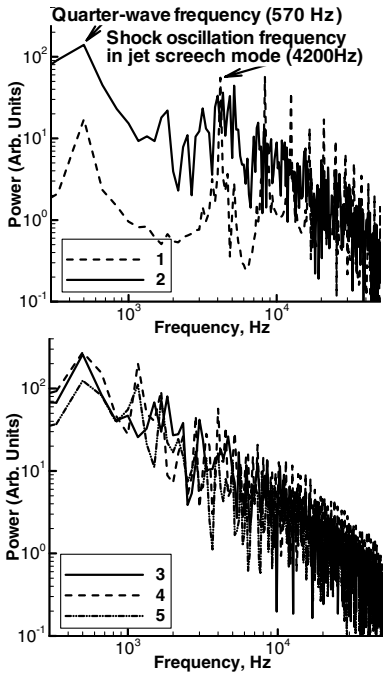

Fig. 7 Fourier analysis of the oscillation inside the resonance tube; configurations 1 and 2 (top) and configurations 3, 4, and 5 (bottom).

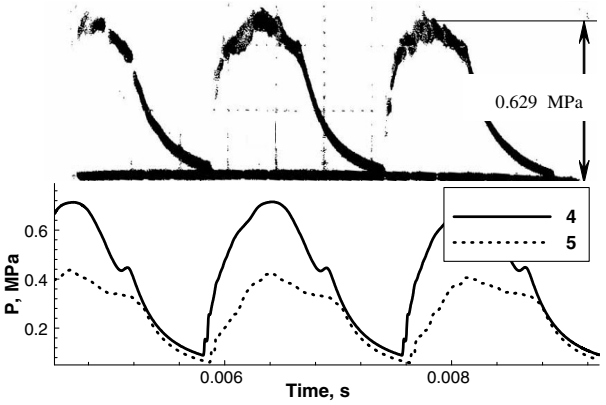

Fig. 8 Comparison of the computed end-wall oscillation (bottom) with experimental measurement [16] (top); configuration 4 (solid line) and configuration 5 (dashed line).

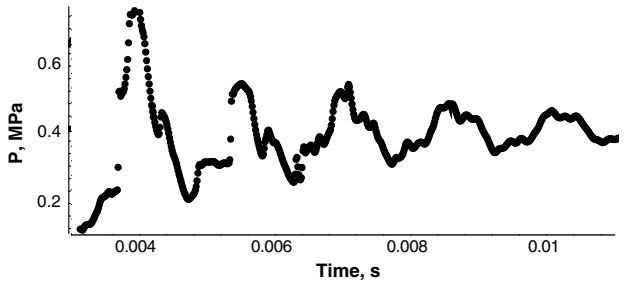

Fig. 9 Decay of induced quarter-wave oscillation in the absence of a needle.

A comparison between measured [16] and computed pressure oscillations on the end wall of the tube is presented in Fig. 8 as a function of time. Computational results for configurations 4 and 5 show pressure amplitudes of 6.3 and 3.8 atm, respectively. Both the amplitude and shape of the computation with the needle ending at the nozzle exit are in excellent agreement with the experimental pressure-time curve for which the amplitude was 0.629 MPa. The needle in the experiments extended slightly beyond the tube exit [16].

As a final verification that the quarter-wave mode cannot be supported in the Hartmann–Sprenger tube in the absence of a needle, we present in Fig. 9 the transient response of the pressure at the midpoint of the tube to a strong initial pulse. At early times, the quarter-wave mode is strongly observed, but it quickly decays to zero and is slowly replaced by a stable high-frequency screech mode of relatively low amplitude, compared with the initial transient. Continued processing of the case shown in Fig. 9 eventually leads to the stationary high-frequency oscillations shown in Fig. 6. Similar transient calculations show a relatively rapid transition to a stationary oscillation when a needle is present on the axis.

C. Flowfield Structure in the Presence of Regurgitant and Screech Modes

The results in the previous section indicate the importance of the needle on the frequency and amplitude of the oscillations. In this section, we compare the details of the flowfield structure of the regurgitant oscillation with that of the screech mode in the absence of a needle (configuration 1) to provide some understanding of the manner in which the needle affects the flowfield.

Pressure and Mach number contours in the region between the nozzle exit plane and the tube inlet are given in Fig. 10 for four equally spaced times during one period of the regurgitant oscillation that is set up in configuration 4 with the needle extending to the exit of the nozzle. In each of the four realizations, the pressure contours are given in the upper half of the plot and the Mach number contours in the lower half. Streamlines are superimposed on the Mach number contours to help understand the flow dynamics. In all four plots, a shock that responds to the dynamics of the flow can be seen in front of the mouth of the tube. Detailed study of other times during the period indicates that the shock is never completely swallowed, but during the compression phase of the oscillation, a second shock enters the tube, propagates to the closed end and reflects, to provide the pressure maximum observed in the preceding figures. Upon reaching the open end of the tube, the reflected shock produces an expansion that evacuates the tube in preparation for the next compression. To enhance the details of the flow near the inlet, this compression/expansion process inside the tube is not included in the figures. Additional details of the flow at these four time instants is given in Fig. 11, which shows cross-stream profiles of the stagnation pressure and axial velocity at six equally spaced intervals between the nozzle exit and the tube inlet.

The first plot in Fig. 10 corresponds to the time at which the compression shock inside the tube (not visible in these plots) is

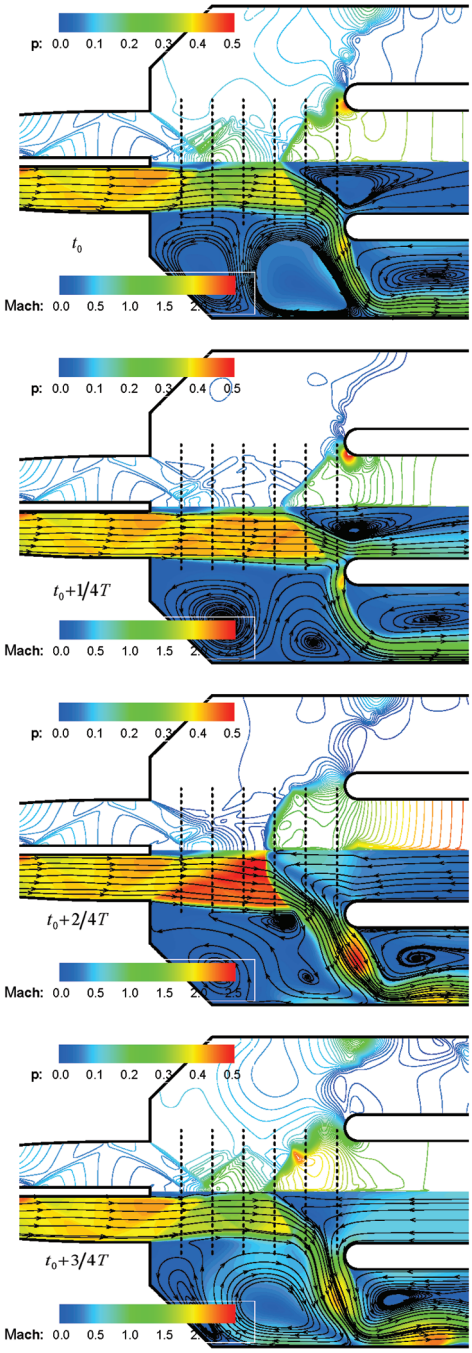

Fig. 10 Flow structure at four equally spaced times in a period during regurgitant operation.

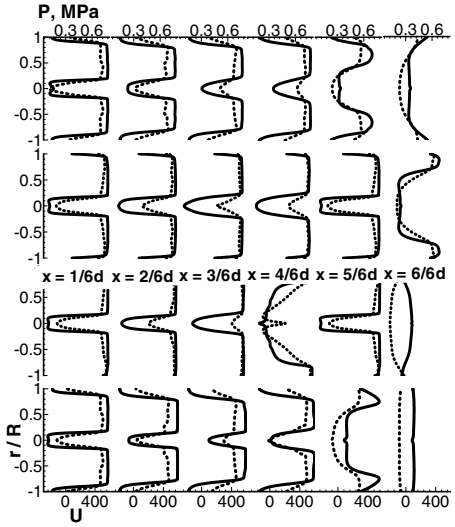

Fig. 11 Stagnation pressure and velocity profiles at six equally spaced locations between the nozzle exit and tube inlet at four times; stagnation pressure (solid line) and axial velocity (dashed line); from the top: $t = t_0$, $t = t_0 + T/4$, $t = t_0 + T/2$, and $t = t_0 + 3/4T$.

approximately halfway to the closed end. The upstream end of the tube is therefore at a relatively high pressure, and the external shock is oblique to the flow. This oblique shock diverts most of the incoming flow around the tube and into the annular passage between the tube and the shroud. The streamlines in this first plot also indicate that there is a recirculation region at the mouth of the tube that creates an interface between the incoming flow and the fluid inside the tube. The velocity profile at the $x = 6/6d$ location indicates that flow is entering the tube only in a narrow region near the wall, but that flow is exiting the tube over most of the diameter.

One-quarter of a period later (the second plot in Figs. 10 and 11), the compression shock inside the tube has reflected from the closed end and is again approximately at the midpoint of the tube. At this time instant, the angle of the external shock has increased such that a larger fraction of the incoming jet is entering the tube. The velocity plot in Fig. 11 shows that the incoming flow is much faster than in the first plot, but both the velocity profile and the streamlines in Fig. 10 indicate that fluid is still flowing out of the tube in the center.

The third and fourth plots in Figs. 10 and 11 correspond to the time after the reflected shock has reached the open end of the tube and expansion waves are traversing the tube to evacuate it. In the first half of the reflection phase (the third plot in Figs. 10 and 11), the shock from inside the tube has reached the exit and pushed the external shock further away from the mouth of the tube so that it is nearly normal to the oncoming stream (probably a strong oblique shock). The high-pressure gases across the entire face of the tube are emptying into the surrounding shroud, along with the mass flow from the nozzle. A companion expansion wave is simultaneously traveling toward the closed end of the tube. The final plot in Fig. 10 shows conditions in which the expansion wave has reflected from the closed end of the tube and is approaching the open end. The tube is nearly evacuated, and the mass replenishment portion of the cycle shown in the first plot is about to begin again. The oblique shock again appears and a slow, nearly uniform outflow occurs across the mouth of the tube.

Details of the flow patterns inside the tube are given in the x–t plots in Fig. 12. The topmost plot shows the pressure variation on the axis of the tube, $r/R = 0$, over approximately two and one-half periods. The left side of the figure corresponds to the open end, and the right side represents the closed end. The corresponding velocity variations for a single cycle (denoted by the dashed lines in the pressure plot) are shown in the bottom three plots for three different radial locations ($r/R = 0, 0.5$, and 0.9). Although there are major radial effects in the velocity plots, the pressure variations on these three radii are essentially the same and, hence, only the $r/R = 0$ results are shown. To indicate flow excursions inside the tube, particle path lines are superimposed on the velocity fields at the three radial locations. Perhaps the most interesting aspect of the path lines is that at the center of the tube (the $r/R = 0$ location), the flow is always outward. Near the middle of the tube, the particles are seen to move over approximately 40% of the tube length, whereas as the closed end is approached, the particle fluctuations decrease to zero.

These results, which reinforce observations from Figs. 10 and 11, indicate that the regurgitant oscillations are dominated by two-dimensional effects. Throughout the cycle, flow exits the tube on the

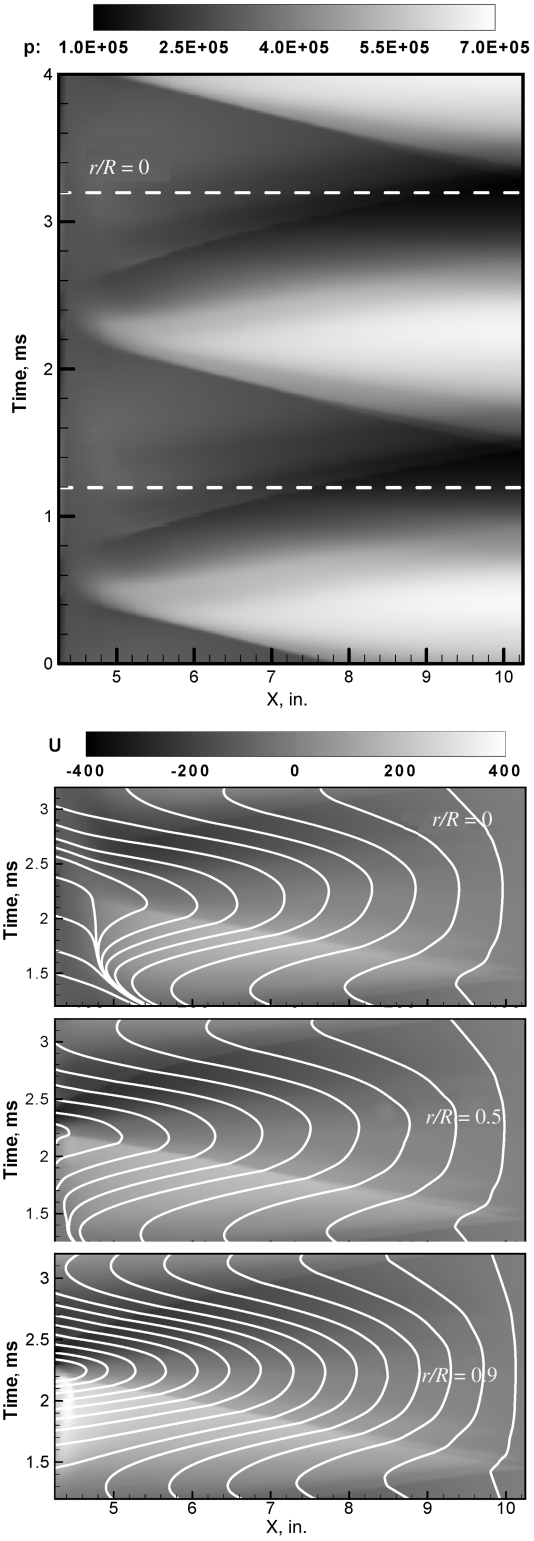

Fig. 12 Inside-tube conditions in the x–t diagram; pressure contours at $r/R = 0$ for 2.5 periods (top) and velocity contours for one period, $r/R = 0$ (second plot), $r/R = 0.5$ (third plot), and $r/R = 0.9$ (bottom).

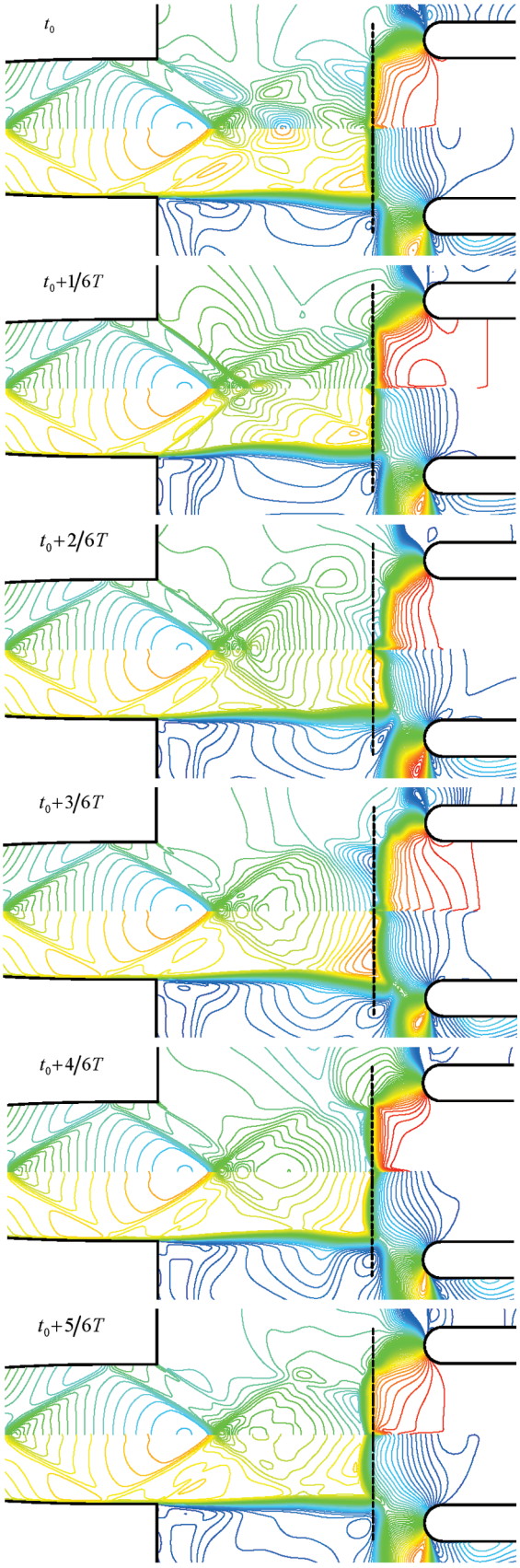

Fig. 13 Pressure (upper) and Mach number (lower) contours in nozzle/tube inlet region at six equally spaced times in a period during screech operation.

centerline, whereas near the outer edges, it vacillates between strong inflow and strong outflow. This strong two-dimensionality, in turn, arises from the stagnation pressure deficit on the axis that is created by the boundary layer from the needle. This pressure deficit is seen in Figs. 4 and 11. Note, in particular, that as the shock wave approaches the normal condition (the third of the four times in Fig. 11), the stagnation pressure deficit from the needle wake is augmented by the shock losses and produces a very wide pressure deficit. Also note that the subsonic flow in the needle wake is affected by the regurgitant oscillation all the way to the needle.

Plots for the screech-mode oscillation (corresponding to configuration 1 without the needle) are given in Figs. 13 and 14. Figure 13 presents contour plots of the pressure (top half) and Mach number (bottom half) for six equally spaced times during the period of the screech oscillation. The shock structure and the flowfield in these plots are dramatically different from those for the regurgitant oscillation. The contour lines show a nearly normal shock sitting outside the tube at all times, but there are essentially no contours inside the tube, indicating that the level of pressure oscillations in the tube is considerably smaller than in the regurgitant mode case. Comparison of the six plots indicates that the shock position does oscillate slightly. To clarify this movement, a vertical dashed line has been placed on each plot to denote the time-averaged position of the shock.

The six realizations indicate that the flow is less organized than in the regurgitant mode, but the concentration of Mach number and pressure contours at the entrance to the nozzle varies from plot to plot, indicating the presence of weak compression and rarefaction waves. Inspection of the flow at the mouth of the tube shows that it is nearly one-dimensional in character throughout the cycle and that the strong inflow and outflow characteristics of the regurgitant cycle are not seen.

A pressure/Mach number plot showing streamlines (analogous to Fig. 10) and the stagnation pressure and velocity profiles (analogous to Fig. 11) is given in Fig. 14 for the time corresponding to the fourth plot in Fig. 13. This plot again shows that the bow shock causes the flow to deviate around the tube and into the passage between the tube and the shroud. Although only one time is shown, conditions throughout the screech oscillation are qualitatively like this. Also note the much more uniform stagnation pressure profiles in front of the tube. For the screech oscillation (without the needle), the flow in front of the shock remains unchanged throughout the cycle.

III. Conclusions

The effect of a needle on the flowfield in a Hartmann–Sprenger tube driven by the supersonic exhaust from a nearly uniformly expanded convergent–divergent nozzle has been investigated by means of computational solutions. The numerical results are based on simulations of the Navier–Stokes equations coupled with a two-equation turbulence model. The needle length has been varied

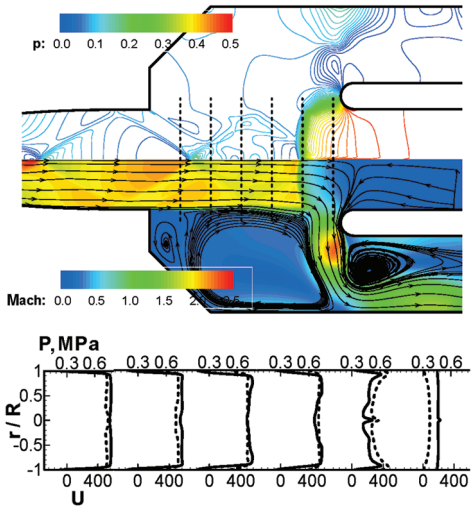

Fig. 14 Pressure (upper) and Mach number (lower) contours in screech with stagnation pressure and velocity profiles at six equally spaced locations; stagnation pressure (solid line) and axial velocity (dashed line).

parametrically for a single nozzle/resonance-tube geometry. Results are presented for oscillations without a needle and for needles of several lengths.

Comparisons of the nozzle and exhaust flow in the absence of a resonance tube show a weak Mach diamond pattern that is essentially unaffected by the presence of a needle. Computations with the resonance tube present, however, show considerable differences. When the needle is not present, the jet flow sets up a screech-mode oscillation that is characterized by high-frequency oscillations of a normal shock sitting in front of the open end of the tube. The addition of a needle amplifies the quarter-wave mode at the expense of the high-frequency modes. The results suggest a gradual transition from screech to regurgitant mode as the needle length is increased, but the presence of even the shortest needle strongly favors the regurgitant mode. Extending the needle beyond the nozzle exit appears to decrease the intensity of the oscillations. The mode frequencies, amplitudes, and wave shapes are shown to be in good quantitative agreement with measurements.

Flowfield details show that the reduced momentum near the axis created by the wake of the needle induces strong two-dimensional effects in the entrance region of the tube while also impacting the shock shape. The reduced velocity in the central part of the oncoming stream allows outflow to occur near the centerline throughout the cycle, whereas the outer portion of the tube experiences periodic inflow and outflow. This low-speed region also induces an oblique shock in front of the tube that turns the flow radially outward to provide the two-dimensional flow. When the needle is not present, the shock resembles a bow shock that oscillates forward and back throughout the cycle, and the inflow/outflow characteristics are much more uniform.

Acknowledgments

Portions of this work were sponsored by the NASA John H. Glenn Research Center under grant NNC04GB04G. We are grateful to Jack Wilson of the QSS Group, Inc. and Daniel E. Paxson of the NASA John H. Glenn Research Center for providing experimental results.

References

[1] Hartmann, J., *Danske Matematisk-fysiske Meddeleser*, No. 1, 1919.
[2] Hartmann, J., "On the Production of Acoustic Waves by Means of an Air-Jet of a Velocity Exceeding That of Sound," *Philosophical Magazine*, No. 11, 1931, pp. 926–948.
[3] Sprenger, H., *Mitteilungen aus dem Institut fur Aerodynamik*, No. 21, 1954, p. 18.
[4] Thompson, P. A., "Jet-Driven Resonance Tube," *AIAA Journal*, Vol. 2, No. 7, 1964, pp. 1230–1233.
[5] Brocher, E., Maresca, C., and Bournay, M.-H., "Fluid Dynamics of Resonance Tube," *Journal of Fluid Mechanics*, Vol. 43, No. 2, 1970, pp. 369–384.
[6] Sarohia, V., and Back, L. H., "Experimental Investigation of Flow and Heating in a Resonance Tube," *Journal of Fluid Mechanics*, Vol. 94, No. 4, 1979, pp. 649–672.
[7] Iwamoto, J., "Necessary Conditions for Starting and Maintaining a Stable Oscillatory Flow in a Hartmann–Sprenger Tube," *Flow Visualization IV*, Hemisphere, Washington, D.C., 1986, pp. 507–512.
[8] Brocher, E., and Duport, E., "Resonance Tubes in a Subsonic Flowfield," *AIAA Journal*, Vol. 26, No. 5, 1988, pp. 548–552.
[9] Vrebalovich, T., "Resonance Tubes in a Supersonic Flow Field," Technical Rept. 32, Jet Propulsion Lab., California Inst. of Technology, Pasadena, CA, 1962, p. 378.
[10] Phillips, B. R., and Pavli, A. J., "Resonance Tube Ignition of Hydrogen–Oxygen Mixtures," NASA TN D6354, May 1971.
[11] Stanek, M. J., Raman, G., Kibens, V., Ross, J., Odedra, J. A., and Peto, J. W., "Suppression of Cavity Resonance Using High Frequency Forcing-The Characteristic Signature of Effective Devices," AIAA/CEAS Aeroacoustics Conference and Exhibit, Maastricht, The Netherlands, AIAA Paper 2001-2128, 2001.
[12] Kastner, J., and Samimy, M., "Development and Characterization of Hartmann Tube Fluidic Actuators for High–Speed Flow Control," *AIAA Journal*, Vol. 40, No. 10, 2002, pp. 1926–1934.
[13] Raman, G., Mills, A., and Kibens, V., "Development of Powered Resonance-Tube Acutators for Aircraft Flow Control Applications," *Journal of Aircraft*, Vol. 41, No. 6, 2004, pp. 1306–1314.
[14] Murugappan, S., and Gutmark, E., "Flowfield and Mixing Control of an Underexpanded Jet," *AIAA Journal*, Vol. 42, No. 8, 2004, pp. 112–1621.
[15] Bogdanoff, D. W., "Advanced Injection and Mixing Techniques for Scramjet Combustors," *Journal of Propulsion and Power*, Vol. 10, No. 2, 1994, pp. 183–190.
[16] Wilson, J., and Paxson, D. E., "Unsteady Ejector Performance: An Experimental Investigation Using a Resonance Tube Driver," 38th AIAA/ASME/SAE/ASEE Joint Propulsion Conference and Exhibit, Indianapolis, IN, AIAA Paper 2002-3632, 2002.
[17] Kim, K.-H., and Chang, K.-S., "Three-Dimensional Structure of a Supersonic Jet Impinging on an Inclined Plate," *Journal of Spacecraft and Rockets*, Vol. 31, No. 5, 1994, pp. 778–782.
[18] Chang, K.-S., Kim, K.-H., and Iwamoto, J., "A Study on the Hartmann–Sprenger Tube Flow Driven by a Sonic Jet," *International Journal of Turbo and Jet Engines*, Vol. 13, No. 3, 1996, pp. 173–182.
[19] Ko, S.-M., and Chang, K.-S., "Resonant Pulsatile Flows of a Hartmann–Sprenger Tube," *Computational Fluid Dynamics Journal*, Vol. 6, No. 4, Jan. 1998, pp. 439–452.
[20] Hamed, A., Das, K., and Basu, D., "Numerical Simulation of Unsteady Flow in Resonance Tube," 40th AIAA Aerospace Sciences Meeting and Exhibit, Reno, NV, AIAA Paper 2002-1118, 2002.
[21] Hamed, A., Das, K., and Basu, D., "Numerical Simulation and Parametric Study of Hartmann–Sprenger Tube Based Power Devices," 41st AIAA Aerospace Sciences Meeting and Exhibit, Reno, NV, AIAA Paper 2003-0550, 2003.
[22] Li, D., Venkateswaran, S., Fakhari, K., and Merkle, C., "Convergence Assessment of General Fluid Equation on Unstructured Hybrid Grids," 15th AIAA Computational Fluid Dynamics Conference, Anaheim, CA, AIAA Paper 2001–2557, 2001.
[23] Wilcox, D. C., *Turbulence Modeling for CFD*, DCW Industries, Inc., La Cãnada, CA, 1998.
[24] Wilson, J., "Vortex Rings Generated by a Shrouded Hartmann–Sprenger Tube," 35th AIAA Fluid Dynamics Conference and Exhibit, Toronto, Ontario, AIAA Paper 2005-5163, 2005.

G. Candler
Associate Editor